CHAPTER

Free Surface and Buoyancy Driven Flows

6

6.1 Introduction

In Chapter 4 we introduced the reader to the solution of incompressible flow problems and illustrated these with many examples of Newtonian (Chapter 4) and non-Newtonian flows (Chapter 5). In the present chapter, we shall address two separate topics of incompressible flow, which were not dealt with in the previous chapters. This chapter is thus divided into two parts. The common theme is that of the action of the body force due to gravity. We start with a section addressed to problems of free surfaces and continue with the second section, which deals with buoyancy effects caused by temperature differences in various parts of the domain.

The first part of this chapter, Section 6.2, deals with problems in which a free surface of flow occurs when gravity forces are acting throughout the domain. Typical examples here would be for instance given by the disturbance of the free surface of water and the creation of waves by moving ships or submarines. Of course other problems of similar kinds arise in practice. Indeed in Chapter 10, where we deal with shallow water flows, a free surface is an essential condition but other assumptions and simplifications have to be introduced. In the present chapter, we shall deal with the full incompressible flow equations without any further physical assumptions. There are other topics of free surfaces which occur in practice. One of these for instance is that of mold filling, which is frequently encountered in manufacturing where a particular fluid or polymer is poured into a mold and solidified.

In Section 6.3, we invoke problems of buoyancy and here we can deal with natural convection when the only force causing the flow is that of the difference between uniform density and density which has been perturbed by a given temperature field. In such examples it is a fairly simple matter to modify the equations so as to deal only with the perturbation forces, but on occasion forced convection is coupled with such naturally occurring convection.

6.2 Free surface flows

6.2.1 General remarks

In many problems of practical importance a free surface will occur in the fluid (always liquid). In general the position of such a free surface is not known and the main problem

Finite Element Meth Fluid Dynam 7E, Volume 3. http://dx.doi.org/10.1016/B978-1-85617-635-4.00006-6

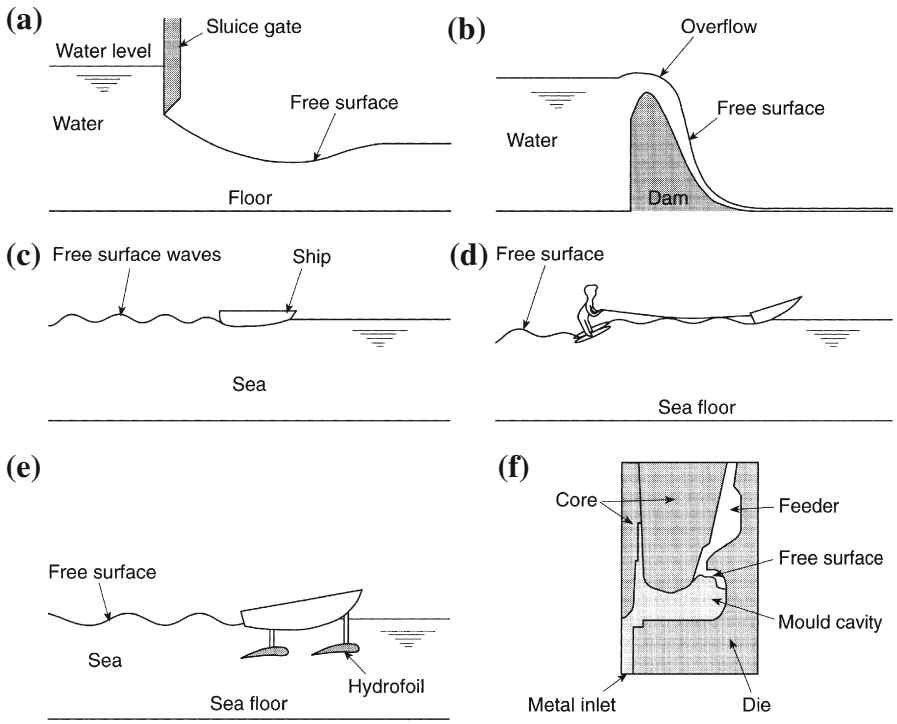

FIGURE 6.1

Typical problems with a free surface.

is that of determining it. In Fig. 6.1, we show a set of typical problems of free surfaces; these range from flow over and under water control structures and flow around ships, to industrial processes such as filling of molds. All these situations deal with a fluid which is incompressible and in which the viscous effects either can be important or on the other hand may be neglected. The only difference from solving the type of problem which we have discussed in the previous two chapters is the fact that the position of the free surface is not known *a priori* and has to be determined during the computation.

There are several ways of dealing with such free surface flows. We broadly classify them into three categories. They are (1) pure Lagrangian methods, (2) Eulerian methods, and (3) arbitrary Lagrangian-Eulerian (ALE) methods.

6.2.1.1 *Lagrangian methods*

In this method we write the equations for the fluid particles whose position is changing continuously in time. Such Lagrangian methods almost always are used in the study of solid mechanics but are relatively seldom applied in fluid dynamics due to the fact that deformation is extremely large in fluids. There is an immediate advantage of Lagrangian formulation in the fact that convective acceleration is nonexistent and

the problem is immediately self-adjoint. Further, for problems in which free surface occurs it allows the free surface to be continuously updated and maintained during the fluid motion [1–9].

6.2.1.2 Eulerian methods

In Eulerian methods for which we have established the equation in Chapter 1 the boundaries of the fluid motion are fixed in position and so indeed are any computational meshes. For free surface problems an immediate difficulty arises as the position of the free surface is not known *a priori*. The numerical method will therefore have to include an additional algorithm to trace the free surface positions [10–24].

6.2.1.3 Arbitrary Langrangian-Eulerian (ALE) methods

With both Lagrangian and Eulerian methods certain difficulties and advantages occur and on occasion it is possible to provide an alternative which attempts to secure the best features of both the Lagrangian and Eulerian descriptions by combining these. Such methods are known as ALE methods. These methods are generally complex to implement and we shall give further description of these methods later [25–43].

6.2.2 Lagrangian method

As mentioned before the mesh moves with the flow in the Lagrangian methods. Thus after completion of the CBS steps involved it is necessary to determine the new positions of the mesh. The fluid dynamics equations solved are the same as the ones presented in Chapter 4 except that the convective terms are absent. The governing equations for isothermal Lagrangian fluid dynamics can be written as

$$\frac{\partial \mathbf{V}}{\partial t} + \frac{\partial \mathbf{G_i}}{\partial x_i} + \mathbf{Q} = 0 \tag{6.1}$$

with

$$\mathbf{V}^{\mathrm{T}} = (\rho, \rho u_j) j = 1, \mathrm{N_{dim}} \tag{6.2}$$

being the independent variable vector, and

$$\mathbf{G}_i^{\mathrm{T}} = (0, -\tau_{ij}) j = 1, \mathrm{N_{dim}} \tag{6.3}$$

where $\mathrm{N_{dim}}$ is the number of spatial dimensions. The source term $\mathbf{Q}$ represents the body force due to gravity.

In the above, the deviatoric stress components τ_{ij} are related to velocity as

$$\tau_{ij} = \mu \left(\frac{\partial u_i}{\partial x_j} + \frac{\partial u_j}{\partial x_i} \right) \tag{6.4}$$

In the above equations, u_i are the velocity components, ρ is the density, p is the pressure, and μ is the dynamic viscosity.

The continuity and dynamic momentum equations are repeated in a detailed indicial form as

Continuity

$$\frac{\partial \rho}{\partial t} + \frac{\partial}{\partial x_i}(U_i) = 0 \tag{6.5}$$

Momentum

$$\frac{\partial U_i}{\partial t} = -\frac{\partial p}{\partial x_i} + \frac{\partial \tau_{ij}}{\partial x_j} + \rho g_i \tag{6.6}$$

where $U_i = \rho u_i$ and g_i is the gravity force. It should be noted that the transient density term in the continuity equation can be replaced by the following relation:

$$\frac{\partial \rho}{\partial t} = \frac{1}{\beta^2}\frac{\partial p}{\partial t} \tag{6.7}$$

where β is an artificial wave speed (Chapter 3). The problem is completed by specifying appropriate initial conditions for u_i and p together with boundary conditions.

The solution procedure follows one of the time discretizations discussed in Chapter 3. For using semi-implicit schemes the transient term is omitted in Eq. (6.5). For fully explicit schemes, this term is retained along with the artificial compressible wave speed [Eq. (6.7)]. However, dual time stepping is necessary when the artificial compressibility method is employed (Chapter 3). The coordinates of the nodes are moved using the following relation after every real time step [3]:

$$x_i^{n+1} = x_i^n + \frac{1}{2}\Delta t(u_i^{n+1} + u_i^n) \tag{6.8}$$

Here Δt is the real time step.

Example 6.1. Lagrangian free surface method for a model broken dam problem

An example problem of a somewhat idealized dam failure as shown in Fig. 6.2 is solved using the semi-implicit form of CBS [44]. Although not realistic, this problem is frequently used as a benchmark for validating Lagrangian algorithms. The experimental data are indeed available and will be used here for comparison. As seen from

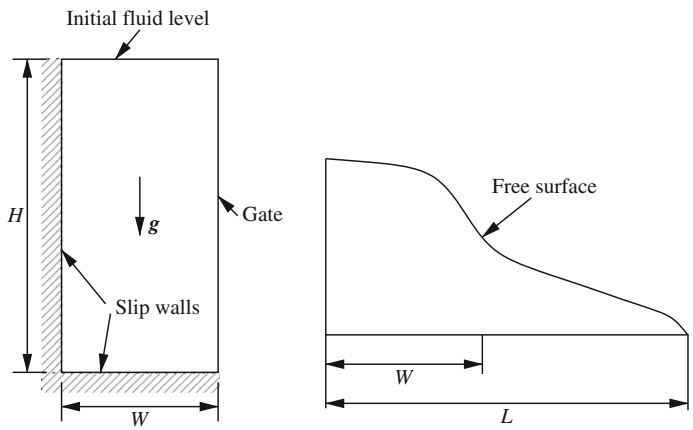

FIGURE 6.2

Broken dam problem. Problem definition and schematic of the free surface.

Fig. 6.2 the problem consists of two slip walls on which slip boundary conditions are applied (normal velocity zero or tangential traction zero). The initial fluid position is as shown in Fig. 6.2 (left) with velocities at all nodes equal to zero. The dimensions of the dam are H = 7 and W = 3.5. The gravity was assumed to act with a magnitude equal to unity (nondimensional). The viscosity was assumed to be 0.01 (nondimensional quantity). At $t = 0$, the gate was opened and the fluid from the dam was assumed to flow freely. The quantity of interest is the extreme horizontal free surface position L as shown in Fig. 6.2 (right). The unstructured mesh used consists of 339 nodes and 604 elements.

Figures 6.3 and 6.4 give the distorted mesh and contours at various time levels. As seen the results are generally smooth all over the domain. The pressure contours are perfect and free of oscillation, which shows the effect of the good pressure stabilization properties of the CBS scheme.

Figure 6.5 shows the comparison of the extreme horizontal position reached by the free surface with the experimental data [45]. As seen the numerical results are in good agreement with the experimental data. The nondimensional time in the horizontal coordinate is calculated as $t\sqrt{2g/\mathrm{W}}$.

Figures 6.3 and 6.4 show how a reasonably regular mesh at $t = 0$ becomes distorted after a certain number of time steps. While the results show a good agreement with

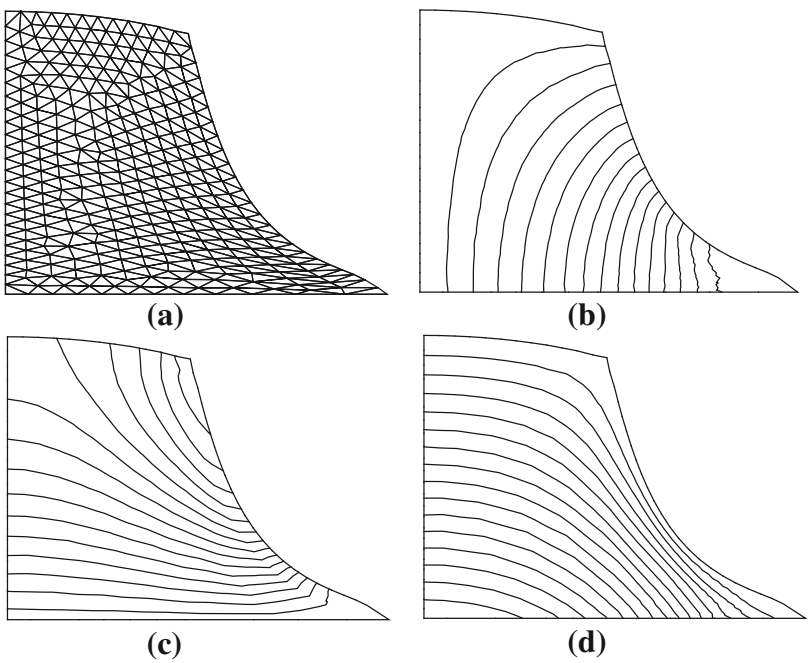

FIGURE 6.3

Broken dam problem. Mesh and contours after $t = 2.0$: (a) mesh; (b) u_1 velocity contours; (c) u_2 velocity contours; (d) pressure contours.

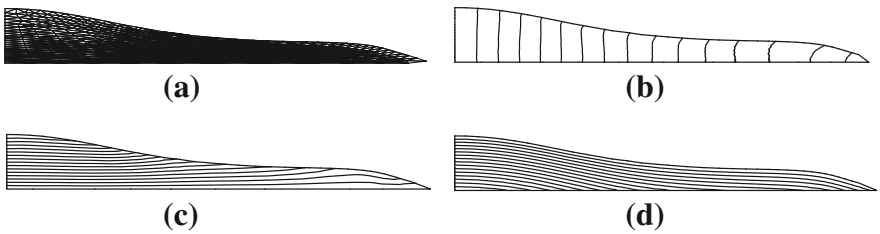

FIGURE 6.4

Broken dam problem. Mesh and contours after $t = 5.0$: (a) mesh; (b) u_1 velocity contours; (c) u_2 velocity contours; (d) pressure contours.

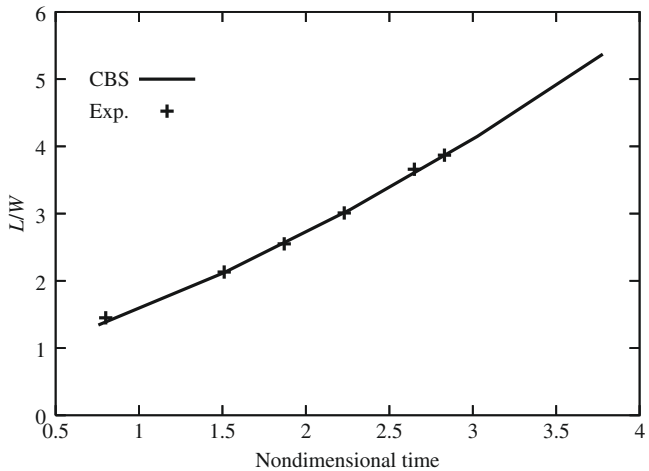

FIGURE 6.5

Broken dam problem. Comparison of numerical results with experimental data [45].

the experimental data the irregularity of the mesh can cause errors and indeed in complicated problems this irregularity may cause element overlapping and *unphysical* results. Here lies one of the serious disadvantages of Lagrangian updating and care has to be taken to avoid extreme errors. Indeed it may be necessary to remesh from time to time the whole problem to avoid element *inversion*. An interesting procedure showing continuous remeshing with a rather novel approach is discussed by Idelshon et al. [46]. We shall not give the details of the procedure here but interested readers should consult appropriate Refs. [47] and [48].

6.2.3 Eulerian methods

As mentioned before the flow domain in Eulerian methods is fixed and the fluid is allowed to pass through the domain. Thus an additional procedure is necessary to track the free surface when Eulerian methods are employed.

In order to correctly track the free surface, we need both dynamic and kinematic conditions to be satisfied on the free surface. Thus, on the free surface we have at all times to ensure that (1) the pressure (which approximates the normal traction) is known (dynamic condition) and (2) that the material particles of the fluid belonging to the free surface remain on this at all times (kinematic condition). These conditions are expressed as

$$\begin{aligned} p &= \overline{p} \\ u_n = \mathbf{n}^{\mathbf{T}}\mathbf{u} &= 0 \end{aligned} \tag{6.9}$$

on the free surface Γ_f. In the above equation u_n is the velocity component in the normal direction to the free surface and $\overline{p}$ is the known pressure. For a non-breaking free surface the kinematic condition (material surface) can be restated for $x_3 = \eta(t, x_1, x_2)$ as

$$\frac{D\eta}{Dt} = u_3 \tag{6.10}$$

or

$$\frac{\partial \eta}{\partial t} + u_1 \frac{\partial \eta}{\partial x_1} + u_2 \frac{\partial \eta}{\partial x_2} - u_3 = 0 \tag{6.11}$$

where u_1, u_2, and u_3 are the velocity components in the x_1, x_2, and x_3 directions shown in Fig. 6.6. At this point it is important to remark that two independent Eulerian approaches in solving free surface flow problems exist. In the first method the free surface is determined by solving Eq. (6.10) along with the dynamic conditions.

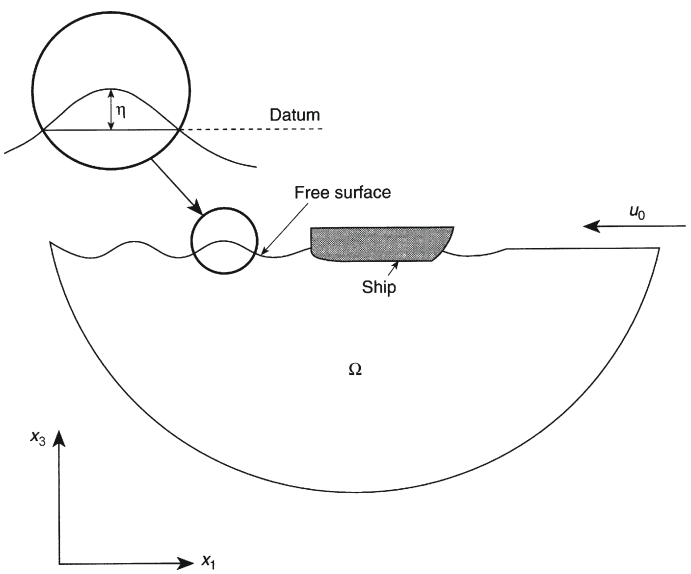

FIGURE 6.6

A typical problem of ship motion.

Once the free surface position η is determined remeshing follows either once at the end of the solution procedure or frequently within the time-stepping iterations. This process of mesh updating is well suited for solving problems of steady-state nature. If this method is employed for the solution of transient problems, some details of the Lagrangian approach need to be included close to the free surface.

In the second Eulerian method the mesh is often fixed throughout the calculation but the free surface is tracked to satisfy the kinematic condition. Once the free surface is tracked the dynamic boundary conditions are applied to satisfy the pressure/traction conditions. The standard procedure used in tracking the free surface is the so-called volume of fluid (VOF) method or one of its variants [10,18,49–52]. The major drawback of this method is that a rough idea about the external free surface is necessary *a priori* in order to generate a mesh which contains the free surface all the time. The VOF-based Eulerian methods are more suitable for internal flows than large-scale external flows.

6.2.3.1 Mesh updating or regeneration methods

Figure 6.6 shows a typical problem of ship motion together with the boundaries limiting the domain of analysis. This is an example of an external free surface flow problem. In the interior of the domain we can use either the full Navier-Stokes equations or, neglecting viscosity effects, a pure potential or Euler approximation. Both assumptions have been discussed in previous chapters but it is interesting to remark here that the resistance caused by the waves may be four or five times greater than that due to viscous drag. Clearly surface effects are of great importance for ship design.

Historically many solutions that ignore viscosity totally have been used in the ship industry with good effect by involving so-called boundary solution procedures or panel methods [53–63]. Early finite element studies on the field of ship hydrodynamics have also used potential flow equations [64]. A full description of these is given in many papers. However complete solutions with viscous effects and full nonlinearity are difficult to deal with. In the procedures that we present in this section, the door is opened to obtain a full solution without any extraneous assumptions and indeed such solutions could include turbulence effects, etc. The nondimensional form of the incompressible flow equations can be written as

$$\frac{\partial u_i}{\partial x_i} = 0 \tag{6.12}$$

and

$$\frac{\partial u_i}{\partial t} + \frac{\partial (u_i u_j)}{\partial x_j} = -\frac{\partial p}{\partial x_i} + \frac{1}{Re}\frac{\partial^2 u_i}{\partial x_i^2} - \frac{x_3}{Fr^2} \tag{6.13}$$

The viscous term in the above equation is simplified using the conservation of mass Eq. (6.12). In the above equations Re is the Reynolds number defined in Chapters 3 and 4 and Fr is the Froude number given as

$$Fr = \frac{u_\infty}{\sqrt{gL}} \tag{6.14}$$

where u_∞ is a reference velocity and L is a reference length.

Further details of the equations can be found in Section 4.1 of Chapter 4 and indeed the same CBS procedure can be used in the solution. However, considerable difficulties arise on the free surface, despite the fact that on such a surface normal traction is known. The difficulties are caused by the fact that at all times we need to ensure that this surface is a material one and contains the particles of the fluid.

Equation (6.11) for free surface height η is a pure convection equation (see Chapter 2) in terms of the variables t, u_1, u_2, and u_3 in which u_3 is a source term. At this stage it is worthwhile remarking that this surface equation has been known for a very long time and was dealt with previously by upwind differences, in particular those introduced on a regular grid by Dawson [54]. However in Chapter 2, we have already discussed other perfectly stable, finite element methods, any of which can be used for dealing with this equation. In particular the characteristic-Galerkin procedure can be applied most effectively.

On occasion additional artificial dissipation is added to stabilize the convection equation (6.11) in its discrete form at the inlet and exit of the domain [16].

It is important to observe that when the steady state is reached we simply have

$$u_3 = u_1 \frac{\partial \eta}{\partial x_1} + u_2 \frac{\partial \eta}{\partial x_2} \tag{6.15}$$

which ensures that the velocity vector is tangential to the free surface. The solution method for the whole problem can now be fully discussed.

The first of these solutions is that involving *mesh updating*, where we proceed as follows. Assuming a known reference surface, say the original horizontal surface of the water, we specify that the pressure on this surface is zero and solve the resulting fluid mechanics problem by the methods of the previous chapter. Using the CBS algorithm we start with known values of the velocities and find the necessary increment obtaining $\mathbf{u}^{\mathbf{n+1}}$ and p^{n+1} from initial values. Immediately following this step we compute the increment of η using the newly calculated values of the velocities. We note here that this last equation is solved only in two dimensions on a mesh corresponding to the projected coordinates of x_1 and x_2 (Figure 6.6).

At this stage the surface can be immediately updated to a new position which now becomes the new reference surface and the procedure can then be repeated to steady state.

6.2.3.2 Hydrostatic adjustment

Obviously the method of repeated mesh updating can be extremely costly and in general we follow the process described as *hydrostatic adjustment*. In this process we note that once the incremental η has been established, we can adjust the surface pressure at the reference surface by

$$p_{ref} = \overline{p} + \Delta \eta^n \rho g \tag{6.16}$$

After each time step the above pressure value is forced on the free surface without altering the mesh. Of course this introduces an approximation but this approximation can be quite satisfactorily used for starting the following step.

If we proceed in this manner until the solution of the basic flow problem is well advanced and the steady state has nearly been reached we have a solution which is reasonably accurate for small waves but which can now be used as a starting point of the mesh adjustment if so desired.

In all practical calculations it is recommended that many steps of the *hydrostatic adjustment* be used before repeating the *mesh updating*, which is quite expensive. In many ship problems it has been shown that with a single mesh quite good results can be obtained without the necessity of proceeding with mesh adjustment. We shall refer to such examples later.

The methodologies suggested here follow the work of Hino et al. [65–67], Idelsohn et al., Löhner et al., and Oñate et al. [17,13,16,21]. The methods which we discussed in the context of ships here provide a basis on which other free surface problems can be started at all times and are obviously an improvement on a very primitive adjustment of the surface by trial and error.

6.2.3.3 Numerical examples using mesh regeneration methods

Example 6.2. A submerged hydrofoil

We start with the two-dimensional problem shown in Fig. 6.7, where a NACA0012 aerofoil profile is used in submerged form as a hydrofoil, which could in the

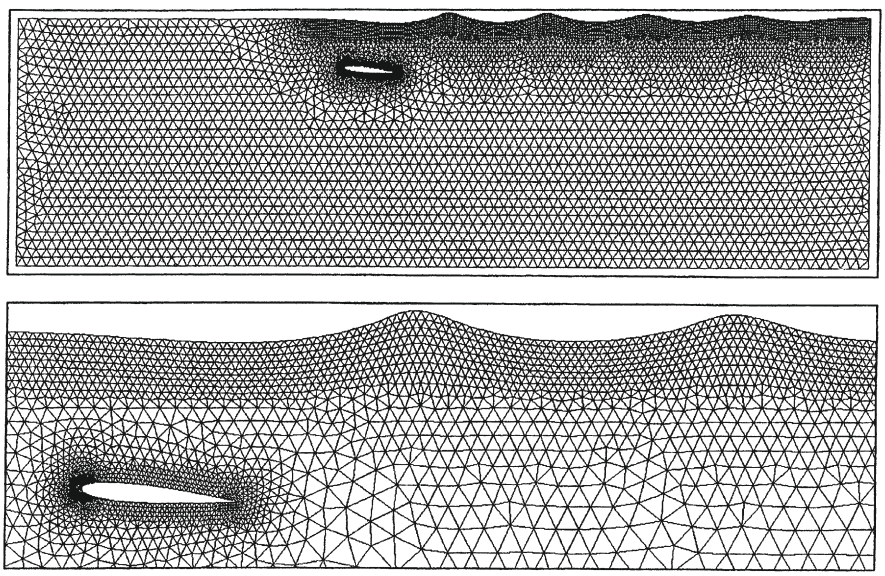

FIGURE 6.7

A submerged hydrofoil. Mesh updating procedure. Euler flow. Mesh after 1900 iterations.

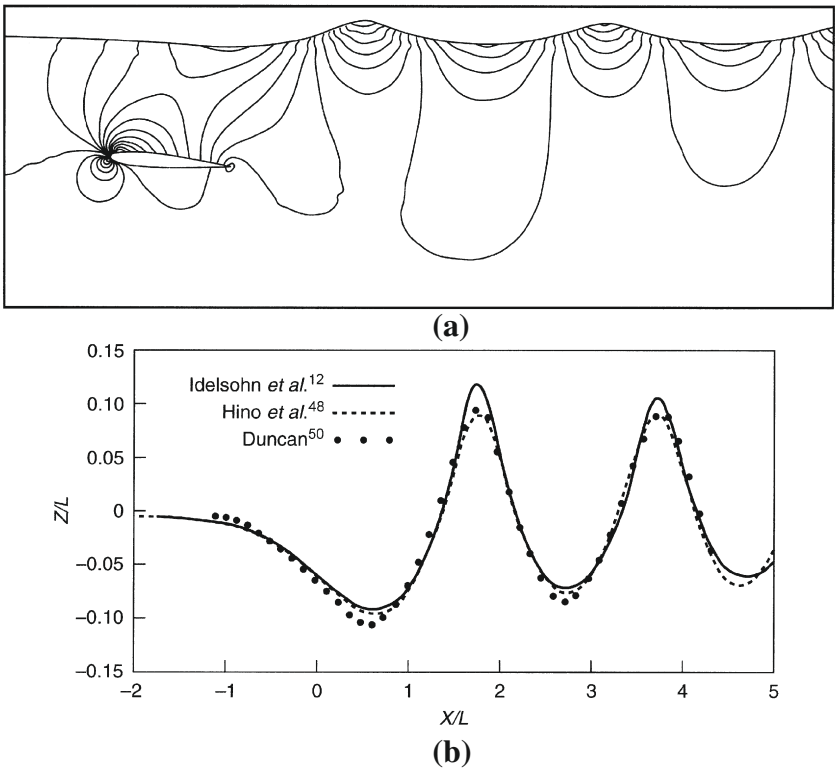

FIGURE 6.8

A submerged hydrofoil. Mesh updating procedure. Euler flow: (a) pressure distribution; (b) comparison with experiment.

imagination of the reader be attached to a ship. This is a model problem, as many two-dimensional situations are not realistic. Here the angle of attack of the flow is 5° and the Froude number is 0.5672.

In Fig. 6.8 we show the pressure distribution throughout the domain and the comparison of the computed wave profiles with the experimental [68] and other numerical solutions [66]. In Figs. 6.7 and 6.8, the mesh is moved after a certain number of iterations using an advancing front technique [69].

Figure 6.9 shows the same hydrofoil problem solved now using hydrostatic adjustment without moving the mesh. For the same conditions, the wave profile is somewhat underpredicted by the hydrostatic adjustment (Fig. 6.9b) while the mesh movement overpredicts the peaks (Fig. 6.8b).

In Fig. 6.10, the results for the same hydrofoil in the presence of viscosity are presented for different Reynolds numbers. As expected the wake is now strong as seen from the velocity magnitude contours (Fig. 6.10a–d). Also at higher Reynolds

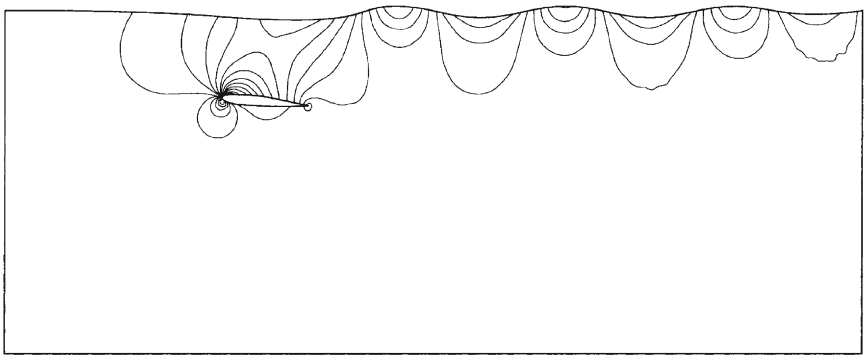

(a)

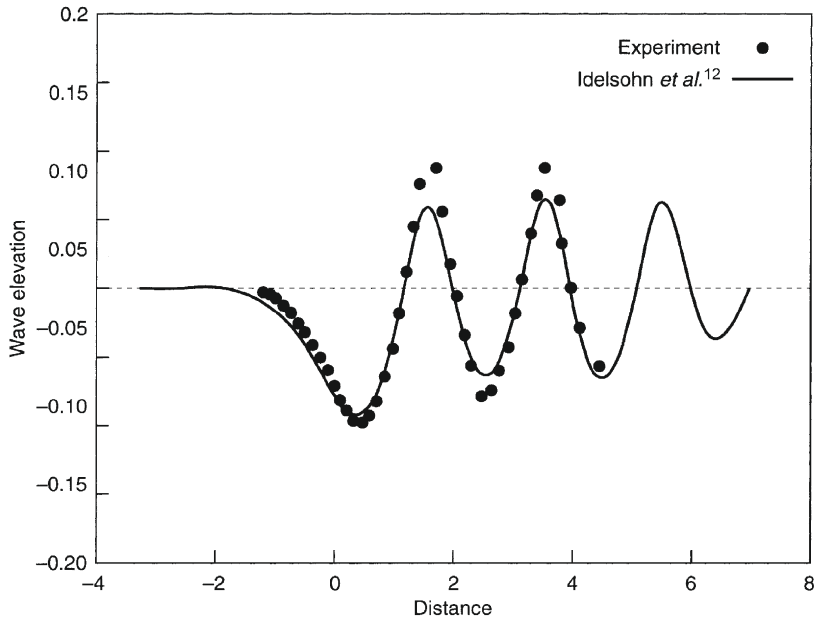

(b)

FIGURE 6.9
A submerged hydrofoil. Hydrostatic adjustment. Euler flow: (a) pressure contours and surface wave pattern; (b) comparison with experiment [68].

numbers (5000 and above), the solution is not stable behind the aerofoil and here an unstable vortex street is predicted as shown in Fig. 6.10c and 6.10d. Figure 6.10e shows the comparison of wave profiles for different Reynolds numbers.

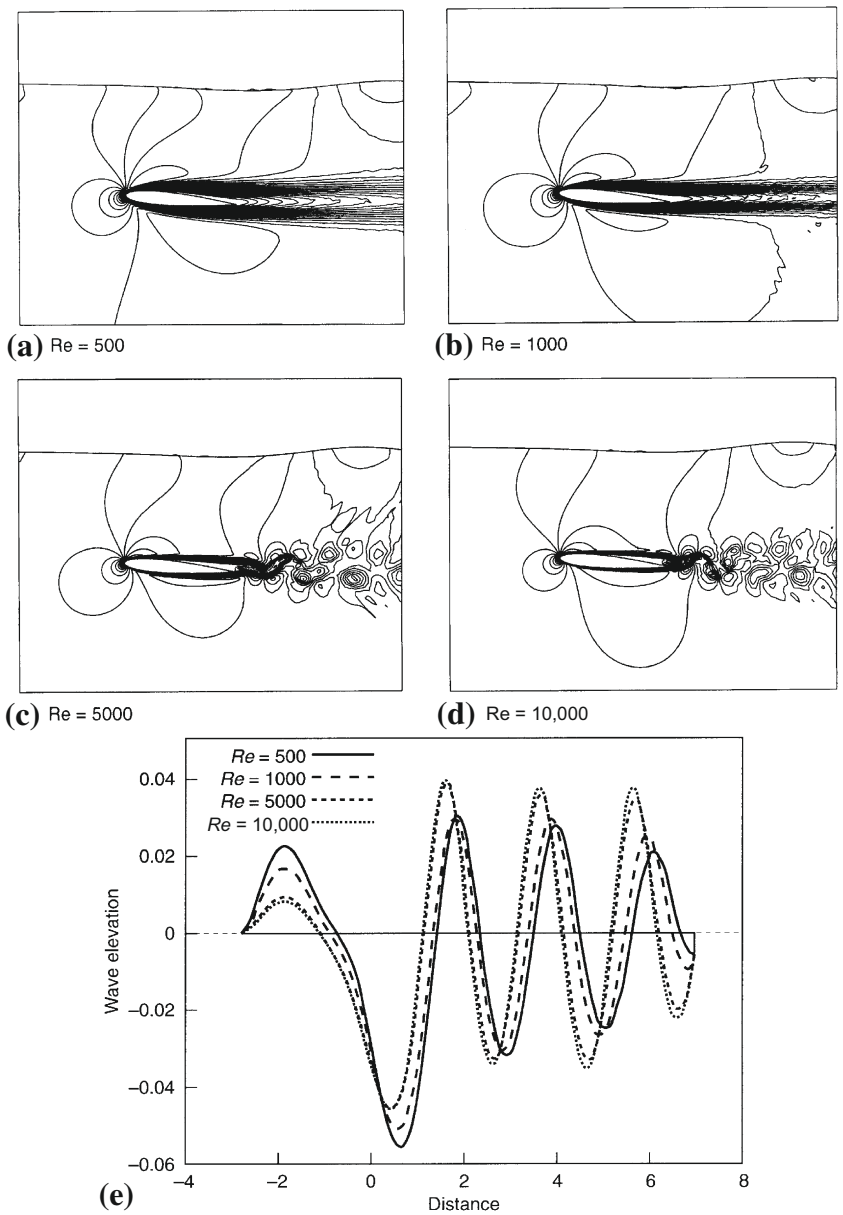

FIGURE 6.10

A submerged hydrofoil. Hydrostatic adjustment. Navier-Stokes flow: (a)–(d) magnitude of total velocity contours for different Reynolds numbers; (e) wave profiles for different Reynolds numbers.

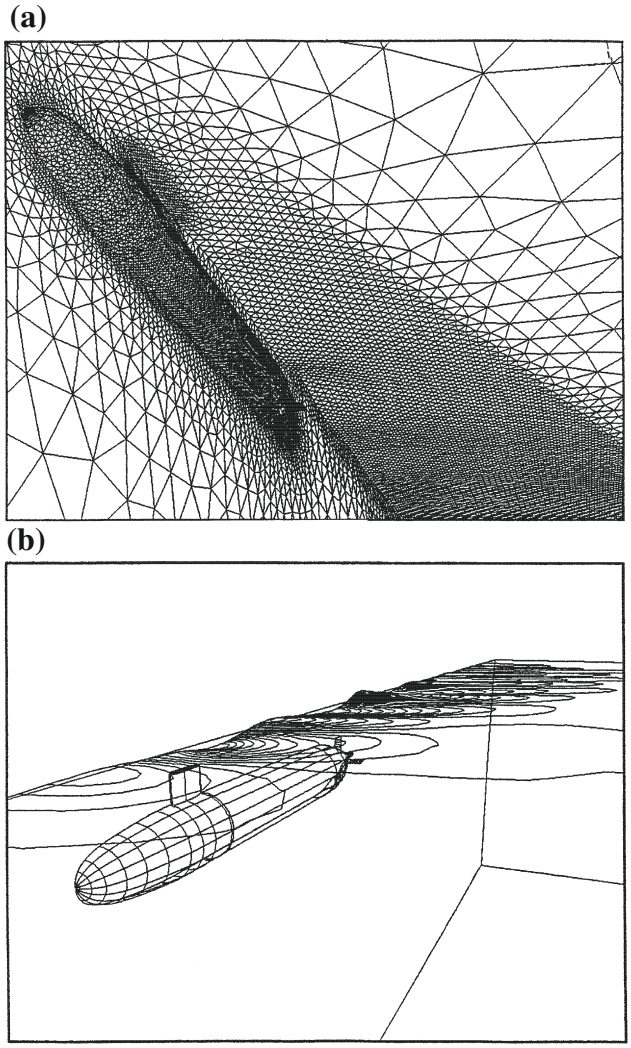

FIGURE 6.11

Submerged DARPA submarine model: (a) surface mesh; (b) wave pattern.

Example 6.3. Submarine

In Fig. 6.11, we show the mesh and wave pattern contours for a submerged DARPA submarine model. Here the Froude number is 0.25. The converged solution is obtained by about 1500 time steps using a parallel computing environment. The mesh consists of approximately 321,000 tetrahedral elements.

Example 6.4. Sailing boat

The last example presented here is that of a sailing yacht. In this case the yacht has a 25° heel angle and a drift angle of 4°. Here it is essential to use either the Euler or Navier-Stokes equations to satisfy the Kutta-Joukoski condition as the potential form has difficulty in satisfying these conditions on the trailing edge of the keel and rudder.

Here we used the Euler equations to solve this problem. Figure 6.12a shows a surface mesh of hull, keel, bulb, and rudder. A total of 104,577 linear tetrahedral elements were used in the computation. Figure 6.12b shows the wave profile contours corresponding to a sailing speed of 10 knots.

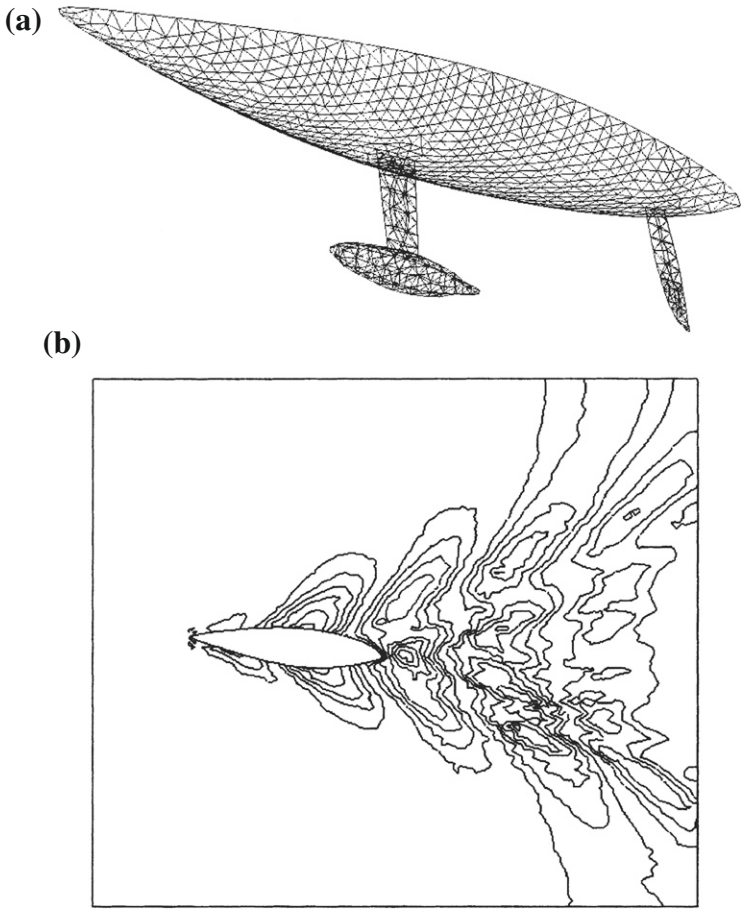

FIGURE 6.12

A sailing boat: (a) surface mesh of hull, keel, bulb, and rudder; (b) wave profile.

6.2.4 Arbitrary Langrangian-Eulerian (ALE) method

As mentioned before ALE methods have some features of both Lagrangian and Eulerian methods. First, let us deal with the basics of the ALE description of flow (for a alternative description see Ref. [39]). Assume a scalar convection-diffusion equation of the form

$$\frac{D\phi}{Dt} = \frac{\partial}{\partial x_i}\left(k\frac{\partial \phi}{\partial x_i}\right) \tag{6.17}$$

where D/Dt is the total time derivative.

Let ϕ be transported to a new position P_f in a time increment of Δt with a velocity of $\mathbf{u}$ as shown in Fig. 6.13 [31]. The ALE method allows independent movement of grid points, i.e., the grid point is moved to a new position P_r in the time increment Δt with a velocity of $\mathbf{u}_g$. The scalar variable ϕ at $t + \Delta t$ at position P_f may be expressed using Taylor series expansion (in both space and time) as

$$\phi_{P_f} = \phi^{n+1} = \phi_P + \Delta t\frac{\partial \phi}{\partial t} + u_i \Delta t\frac{\partial \phi}{\partial x_i} + \cdots \tag{6.18}$$

where u_i are the convective velocity components. In a similar fashion ϕ at position P_r at time t may be expanded (only in space) as

$$\phi_{P_r} = \phi^{n} = \phi_P + u_{gi} \Delta t\frac{\partial \phi}{\partial x_i} + \cdots \tag{6.19}$$

Here u_{gi} are the grid velocity components. The relative value of the scalar variable ϕ with respect to the reference point P_r may be written as

$$\Delta\phi = \phi^{n+1} - \phi^{n} = \Delta t\frac{\partial \phi}{\partial t} + (u_i - u_{gi})\Delta t\frac{\partial \phi}{\partial x_i} \tag{6.20}$$

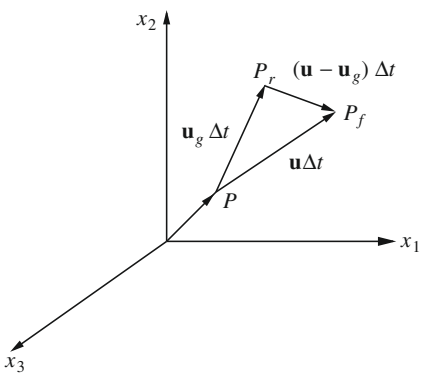

FIGURE 6.13

ALE description in Cartesian coordinates.

The above equation may be rewritten as $\Delta t \to 0$ as

$$\frac{D\phi}{Dt} = \frac{\partial \phi}{\partial t} + (u_i - u_{gi})\frac{\partial \phi}{\partial x_i} \tag{6.21}$$

Substituting Eq. (6.21) into Eq. (6.17) gives the following equation in an ALE framework:

$$\frac{\partial \phi}{\partial t} + (u_i - u_{gi})\frac{\partial \phi}{\partial x_i} - \frac{\partial}{\partial x_i}\left(k\frac{\partial \phi}{\partial x_i}\right) = 0 \tag{6.22}$$

Similarly the incompressible fluid dynamics equations in terms of total derivatives can be written as (for simplicity it is written in terms of primitive variables)
Continuity

$$\frac{D\rho}{Dt} + \rho\frac{\partial u_i}{\partial x_i} = 0 \tag{6.23}$$

Momentum

$$\frac{Du_i}{Dt} = -\frac{1}{\rho}\frac{\partial p}{\partial x_i} + \frac{1}{\rho}\frac{\partial \tau_{ij}}{\partial x_j} - g_i \tag{6.24}$$

The ALE settings for the incompressible flows can be written as
Continuity

$$\frac{\partial \rho}{\partial t} + (u_i - u_{gi})\frac{\partial \rho}{\partial x_i} + \rho\frac{\partial u_i}{\partial x_i} = 0 \tag{6.25}$$

Momentum

$$\frac{\partial u_i}{\partial t} + (u_i - u_{gi})\frac{\partial u_i}{\partial x_i} = -\frac{1}{\rho}\frac{\partial p}{\partial x_i} + \frac{1}{\rho}\frac{\partial \tau_{ij}}{\partial x_j} + g_i \tag{6.26}$$

For constant density flows the continuity equation becomes

$$\frac{\partial u_i}{\partial x_i} = 0 \tag{6.27}$$

It is easy to observe that Eq. (6.26) becomes a Lagrangian equation if grid velocity u_{gi} is equal to fluid velocity u_i and it becomes an Eulerian equation if $u_{gi} = 0$. Thus using an ALE method it is possible to shift between the Lagrangian and Eulerian frameworks if necessary.

6.2.4.1 ALE implementation

As mentioned before implementation of the ALE method is difficult and varies depending on the problem to be solved. However, many have used this method to solve free surface problems with relatively small free surface displacement [25–27,29,31,33–40,44]. The most difficult problem in an ALE algorithm is allocating an appropriate mesh velocity u_{gi}. There is no universal method of determining the mesh velocity. Most of the time mesh velocity is problem dependent. It is standard practice

in ALE algorithms to split the scheme into three phases. They are (1) Lagrangian solution, (2) mesh rezoning action, and (3) Eulerian calculation. However, these phases are seldom discriminated in a computer code.

The ALE procedure starts with a Lagrangian step as discussed in Section 6.2.2. If the mesh is expected to undergo too much distortion then a mesh rezoning procedure should be employed. There are various ways of rezoning available, including remeshing. Once the rezoning is carried out a mesh velocity can be calculated from the nodal displacements to use it in the calculation of the convection velocity in Eq. (6.26).

There are several mesh rezoning procedures available for triangular and tetrahedral elements. One such procedure was introduced by Giuliani [70] in which a function is constructed from measures of distortion and squeeze and minimized. This procedure works well for domains with fixed boundaries. Several improvements have been later carried out by many authors [71]. A variable smoothing method based on a combination of Laplacian smoothing and Winslow's method was introduced by Hermansson and Hansbo [72] which preserves the element stretching. It is also possible to use simple smoothing procedures widely employed in mesh generation, for instance a smoothing procedure in which coordinates of a node are recalculated as an average of the coordinates of the surrounding nodes. Depending on the requirements this smoothing procedure can be employed several times within a single time step.

Apart from the simple mesh moving procedures mentioned above, more robust methods can also be employed for complex situations. Some of the methods based on differential equations are described in detail in Chapter 13.

Example 6.5. Solitary wave propagation

We now consider a simple example of a solitary wave propagation between two walls. Figure 6.14 shows the problem definition. It consists of a liquid with free surface constrained within three wall (two vertical walls and one bottom horizontal wall). The total horizontal length of the domain is 16 and $d = 1$. The gravity direction is downward vertical with $g = 9.81$. The viscosity of the fluid is assumed to be 0.01. The time step employed is 0.025.

The walls are assumed to be slip walls and initial conditions are calculated based on the work presented by Laitone [73] for an infinite domain. The relationships for

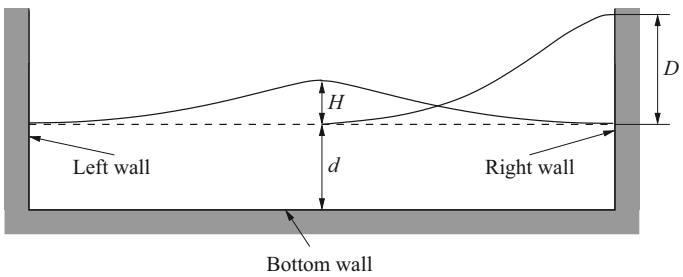

FIGURE 6.14

Solitary wave propagation. Problem definition.

total wave height, velocity components, and pressure are given as

$$h = d + H\text{sech}^2\left[\sqrt{\frac{3H}{4d^3}}(x_1 - ct)\right] \tag{6.28a}$$

$$u_1 = \sqrt{gd}\frac{H}{d}\text{sech}^2\left[\sqrt{\frac{3H}{4d^3}}(x_1 - ct)\right] \tag{6.28b}$$

$$u_2 = \sqrt{3gd}\left(\frac{h}{d}\right)^{3/2}\left(\frac{x_2}{d}\right)\text{sech}^2\left[\sqrt{\frac{3H}{4d^3}}(x_1 - ct)\right]\tanh\left[\sqrt{\frac{3H}{4d^3}}(x_1 - ct)\right] \tag{6.28c}$$

and

$$p = \rho g(h - x_2) \tag{6.28d}$$

In the above equation c is given as

$$\frac{c}{\sqrt{gd}} = 1 + \frac{1}{2}\frac{H}{d} - \frac{3}{20}\left(\frac{H}{d}\right)^2 + \text{O}\left(\frac{H}{d}\right)^3 \tag{6.29}$$

The initial solution and mesh are generated by substituting $t = 0$ into Eqs. (6.28a)–(6.28c).

In Figs. 6.15 and 6.16 we show the meshes and the velocity vectors at various time levels for $H/d = 0.3$. The total number of elements and nodes is unchanged

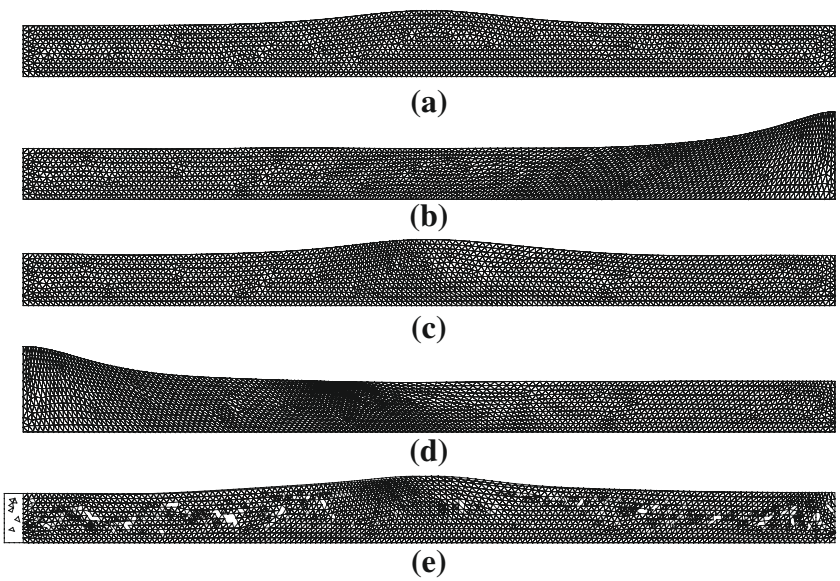

FIGURE 6.15
Solitary wave propagation. Meshes at various time levels: (a) $t = 0.0$; (b) $t = 2.28$; (c) $t = 4.58$; (d) $t = 6.84$; (e) $t = 9.12$.

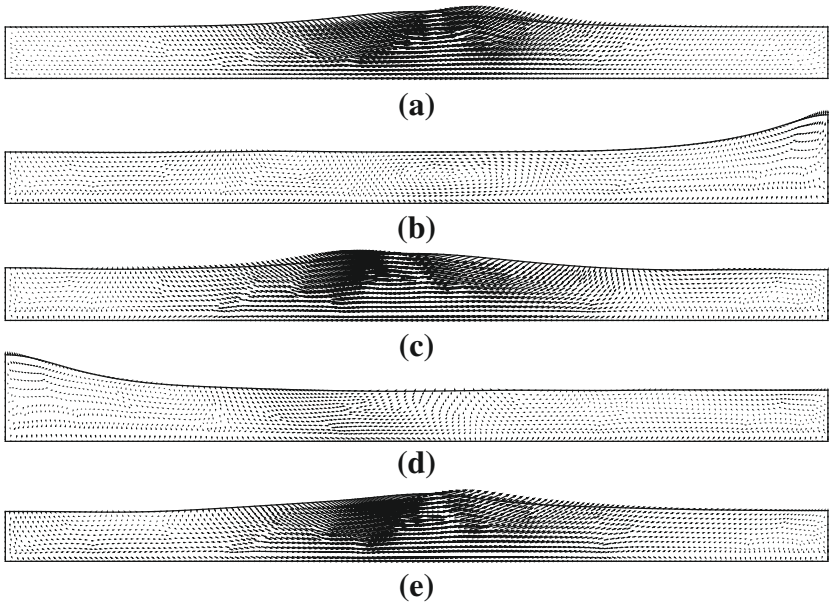

FIGURE 6.16
Solitary wave propagation. Velocity vector distribution at various time levels: (a) $t = 0.0$; (b) $t = 2.28$; (c) $t = 4.58$; (d) $t = 6.84$; (e) $t = 9.12$.

during the calculation; they are 3838 and 2092, respectively. The semi-implicit form of the CBS scheme was used in the calculations. The small portion close to the bottom wall was assumed to be Eulerian all the time. After every time step the Lagrangian portion of the mesh is moved with the fluid and followed by mesh smoothing. The convection term is a part of the ALE scheme. However, during the Lagrangian phase the convection velocity is automatically calculated as equal to zero. However, after

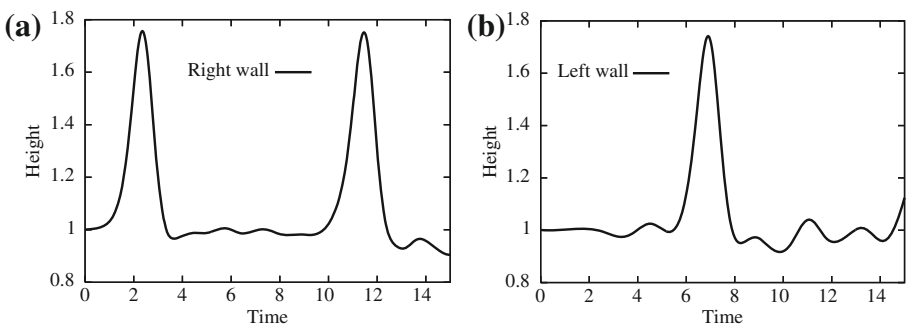

FIGURE 6.17
Wave heights with respect to time on the right and left side walls: (a) right wall; (b) left wall.

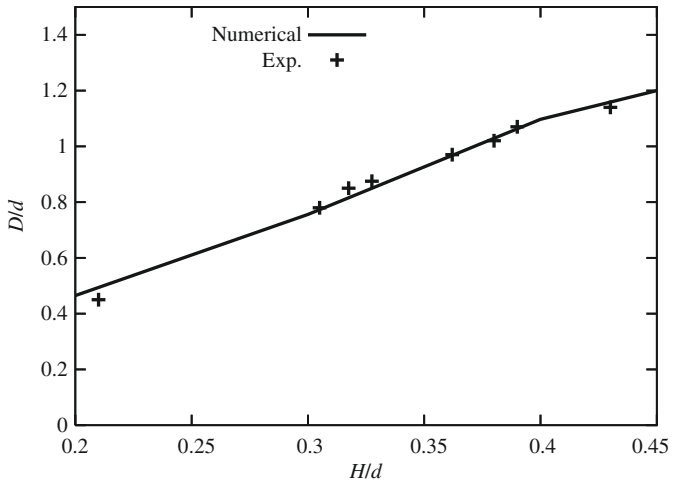

FIGURE 6.18

Solitary wave propagation. Comparison of wave heights with experimental data [74].

the mesh smoothing phase the convection velocity will have a value due to the mesh movement. Note that after mesh smoothing $(u_i - u_{ig})$ will be nonzero on the nodes, which moved relative to the fluid motion.

Figure 6.17 shows the fluid height at the right and left walls with time. As seen the first peak at the right wall is reached around a time of 2.28 and at the left wall the peak is reached at 6.9. Fig. 6.18 shows the comparison of maximum height reached D against the experimental data of Maxworthy [74].

6.3 Buoyancy driven flows

In some problems of incompressible flow the heat transport equation and the equations of motion are weakly coupled. If the temperature distribution is known at any time, the density changes caused by this temperature variation can be evaluated. These may on occasion be the only driving force of the problem. In this situation it is convenient to note that the body force with constant density can be considered as balanced by an initial hydrostatic pressure and thus the driving force which causes the motion is in fact the body force caused by the difference of local density values. We can thus write the body force at any point in the equations of motion as

$$\rho_\infty \left[\frac{\partial u_i}{\partial t} + \frac{\partial}{\partial x_j}(u_j u_i) \right] = -\frac{\partial p}{\partial x_i} + \frac{\partial \tau_{ij}}{\partial x_j} + g_i(\rho - \rho_\infty) \tag{6.30}$$

where ρ is the actual density applicable locally and ρ_∞ is the undisturbed constant density. The actual density entirely depends on the coefficient of thermal expansion of the fluid as compressibility is by definition excluded. Denoting the coefficient of

thermal expansion as γ_T, we can write

$$\gamma_T = \frac{1}{\rho_\infty}\left(\frac{\partial \rho}{\partial T}\right) \tag{6.31}$$

where T is the absolute temperature. The above equation can be approximated to

$$\gamma_T \approx \frac{1}{\rho_\infty}\left(\frac{\rho - \rho_\infty}{T - T_\infty}\right) \tag{6.32}$$

Replacing the body force term in the momentum equation by the above relation we can write

$$\rho_\infty\left[\frac{\partial u_i}{\partial t} + \frac{\partial}{\partial x_j}(u_j u_i)\right] = -\frac{\partial p}{\partial x_i} + \frac{\partial \tau_{ij}}{\partial x_j} + \gamma_T g_i \rho_\infty (T - T_\infty) \tag{6.33}$$

The various governing nondimensional numbers used in the buoyancy flow calculations are the Rayleigh number (for a detailed nondimensionalization procedure see Refs. [75–78])

$$Ra = \frac{g\gamma_T (T - T_\infty)L^3}{\nu\alpha} \tag{6.34}$$

and the Prandtl number

$$Pr = \frac{\nu}{\alpha} \tag{6.35}$$

where L is a reference dimension, and ν and α are the kinematic viscosity and thermal diffusivity respectively and are defined as

$$\nu = \frac{\mu}{\rho}, \qquad \alpha = \frac{k}{\rho c_p} \tag{6.36}$$

where μ is the dynamic viscosity, k is the thermal conductivity, and c_p is the specific heat at constant pressure.

The resulting momentum equation in nondimensional form is

$$\left[\frac{\partial u_i}{\partial t} + \frac{\partial}{\partial x_j}(u_j u_i)\right] = -\frac{\partial p}{\partial x_i} + \frac{\partial \tau_{ij}}{\partial x_j} + n_i Ra\, Pr\, T \tag{6.37}$$

Note that n_i in the above equation is a unit vector in the gravity direction. In many practical situations, both buoyancy and forced flows are equally strong and such cases are often called mixed convective flows. Here in addition to the above-mentioned nondimensional numbers, the Reynolds number also plays a role. The reader can refer to several available basic heat transfer books and other publications to get further details [75, 78–95].

Example 6.6. Buoyancy driven flow in an enclosure

Fundamental buoyancy flow analysis in closed cavities can be classified into two categories. The first one is flow in closed cavities heated from the vertical sides and the second is bottom-heated cavities (Rayleigh-Benard convection). In the former, the CBS algorithm can be applied directly. However, the latter needs some perturbation to start the convective flow as they represent essentially an unstable problem.

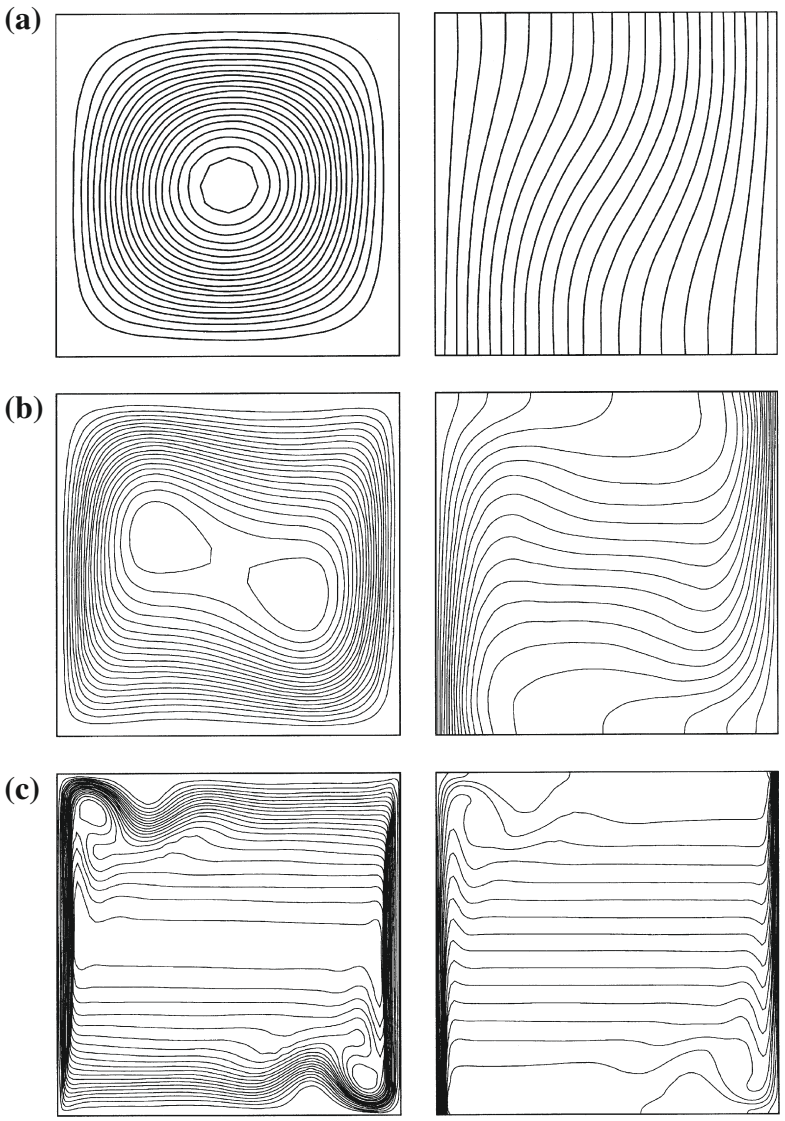

FIGURE 6.19
Natural convection in a square enclosure. Streamlines and isotherms for different Rayleigh numbers. (a) $Ra = 10^4$; (b) $Ra = 10^5$; (c) $Ra = 10^7$.

Figure 6.19 shows the results obtained for a closed square cavity heated at a vertical side and cooled at the other [76]. Both the horizontal sides are assumed to be adiabatic. At all surfaces both of the velocity components are zero (no-slip conditions). The mesh used here was a nonuniform structured mesh of size 51×51.

Table 6.1 Natural Convection in a Square Enclosure. Comparison with Available Numerical Solutions [76]. References Are Shown in Square Brackets

Ra	v			ψmax			$v$max		
	[90]	[91]	CBS	[90]	[91]	CBS	[90]	[91]	CBS
10^3	1.116	1.118	1.117	1.174	1.175	1.167	3.696	3.697	3.692
10^4	2.243	2.245	2.243	5.081	5.074	5.075	19.64	19.63	19.63
10^5	4.517	4.522	4.521	9.121	9.619	9.153	68.68	68.64	68.85
10^6	8.797	8.825	8.806	16.41	16.81	16.49	221.3	220.6	221.6
10^7	–	16.52	16.40	–	30.17	30.33	–	699.3	702.3
4×10^7	–	23.78	23.64	–	–	43.12	–	–	1417

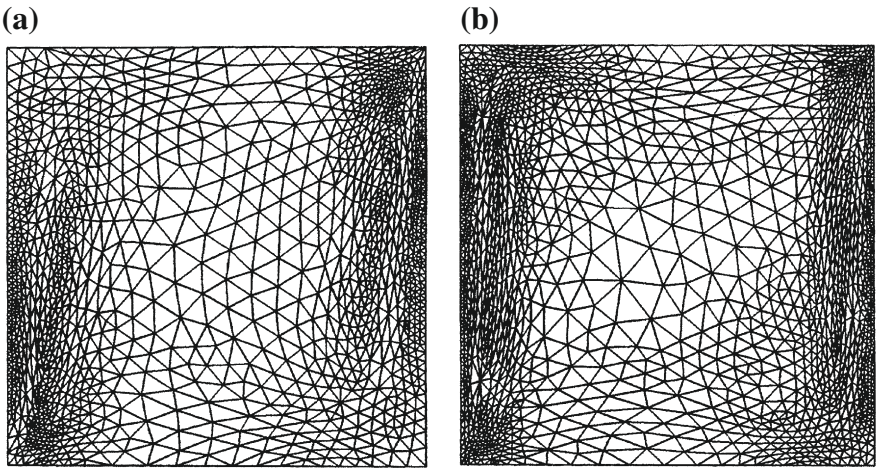

FIGURE 6.20

Natural convection in a square enclosure. Adapted meshes for (a) $Ra = 10^5$ and (b) $Ra = 10^6$.

As the reader can see, the essential features of a buoyancy driven flow are captured using the CBS algorithm. The quantitative results are shown in Table 6.1 [76].

The adapted meshes for two different Rayleigh numbers are shown in Fig. 6.20 The adaptive methods are discussed in Chapter 4 for incompressible flows.

6.4 Concluding remarks

We have summarized all major methods for dealing with free surface flow analysis in this chapter. The numerical formulation of the free surface problems was only briefly discussed. Although brief, we believe that we have provided the readers with some essential technique to start their research on free surface flows. The section on the

buoyancy driven flows is kept purposely brief. Interested readers should consult the quoted references.

References

[1] P. Bach, O. Hassager, An algorithm for the use of the Lagrangian specification in Newtonian fluid mechanics and applications to free-surface flow, J. Fluid Mech. 152 (1985) 173–190.

[2] B. Ramaswamy, M. Kawahara, T. Nakayama, Lagrangian finite element method for the analysis of two dimensional sloshing problems, Int. J. Numer. Methods Fluids 6 (1986) 659–670.

[3] B. Ramaswamy, M. Kawahara, Lagrangian finite element analysis applied to viscous free surface fluid flow, Int. J. Numer. Methods Fluids 7 (9) (1987) 953–984.

[4] M. Hayashi, K. Hatanaka, M. Kawahara, Lagrangian finite element method for free surface Navier-Stokes flow using fractional step methods, Int. J. Numer. Methods Fluids 13 (7) (1991) 805–840.

[5] F. Muttin, T. Coupez, M. Bellet, J.L. Chenot, Lagrangian finite element analysis of time dependent viscous free surface flow using automatic remeshing technique—application to metal casting flow, Int. J. Numer. Methods Engineering 36 (12) (1993) 2001–2015.

[6] Y.T. Feng, D. Peric, A time-adaptive space-time finite element method for incompressible Lagrangian flows with free surfaces: computational issues, Comput. Methods. Appl. Mech. Eng. 190 (5–7) (2000) 499–518.

[7] R. Aubry, S.R. Idelsohn, E. Oñate, Fractional step like schemes for free surface problems with thermal coupling using the Lagrangian PFEM, Comput. Mech. 38 (4–5) (2006) 294–309, 13th Conference on Finite Elements for Flow Problems, Swansea, Wales, APR 04–06 2005.

[8] F. Del Pin, S.R. Idelsohn, E. Oñate, R. Aubry, The ALE/Lagrangian particle finite element method: a new approach to computation of free-surface flows and fluid-object interactions, Comput. Fluids 36 (1) (2007) 27–38.

[9] D. Gonzalez, E. Cueto, F. Chinesta, M. Doblare, A natural element updated Lagrangian strategy for free-surface fluid dynamics, J. Comput. Phys. 223 (1) (2007) 127–150.

[10] C.W. Hirt, B.D. Nichols, Volume of fluid (VOF) method for the dynamics of free surface boundaries, J. Comput. Phys. 39 (1981) 210–225.

[11] J. Farmer, L. Martinelli, A. Jameson, Fast multigrid method for solving incompressible hydrodynamic problems with free surfaces, AIAA J. 32 (1994) 1175–1182.

[12] M. Beddhu, L.K. Taylor, D.L. Whitfield, A time accurate calculation procedure for flows with a free surface using a modified artificial compressibility formulation, Appl. Math. Comput. 65 (1994) 33–48.

[13] R. Löhner, C. Yang, E. Onate, I.R. Idelsohn, An unstructured grid based, parallel free surface solver, AIAA 97–1830 (1997).

[14] G.D. Tzabiras, A numerical investigation of 2D, steady free surface flows, Int. J. Numer. Methods Fluids 25 (1997) 567–598.
[15] J.H. Jeong, D.Y. Yang, Finite element analysis of transient fluid flow with free surface using VOF (volume-of-fluid) method and adaptive grid, Int. J. Numer. Methods Fluids 26 (10) (1998) 1127–1154.
[16] R. Löhner, C. Yang, E. Oñate, Free surface hydrodynamics using unstructured grids, in: 4th ECCOMAS CFD Conference, Athens, September 7–11, 1998.
[17] S.R. Idelsohn, E. Oñate, C. Sacco, Finite element solution of free surface ship wave problems, Int. J. Numer. Methods Eng. 45 (1999) 503–528.
[18] S. Shin, W.I. Lee, Finite element analysis of incompressible viscous flow with moving free surface by selective volume of fluid method, Int. J. Heat Fluid Flow 21 (2000) 197–206.
[19] E.H. van Brummelen, H.C. Raven, B. Koren, Efficient numerical solution of steady free-surface Navier-Stokes flow, J. Comput. Phy. 174 (2001) 120–137.
[20] M.S. Kim, J.S. Park, W.I. Lee, A new VOF-based numerical scheme for the simulation of fluid flow with free surface. Part II: Application to the cavity filling and sloshing problems, Int. J. Numer. Methods Fluids 42 (7) (2003) 791–812.
[21] E. Oñate, J. García, S.R. Idelsohn, Ship hydrodynamics, Encyclophedia Comput. Mech. (2004).
[22] C.L. Lin, H. Lee, T. Lee, L.J. Weber, A level set characteristic Galerkin finite element method for free surface flows, Int. J. Numer. Methods Fluids 49 (5) (2005) 521–547.
[23] C.E. Kees, I. Akkerman, M.W. Farthing, Y. Bazilevs, A conservative level set method suitable for variable-order approximations and unstructured meshes, J. Comput. Phys. 230 (12) (2011) 4536–4558.
[24] R. Rossi, A. Larese, P. Dadvand, E. Onate, An efficient edge-based level set finite element method for free surface flow problems, Int. J. Numer. Methods Fluids 71 (6) (2013) 687–716.
[25] C.W. Hirt, A.A. Amsden, J.L. Cook, An arbitrary Lagrangian-Eulerian computing method for all flow speeds, J. Comput. Phys. 14 (1974) 227–253.
[26] B. Ramaswamy, M. Kawahara, Arbitrary Lagrangian Eulerian finite element method for unsteady, convective incompressible viscous free surface fluid flow, Int. J. Numer. Methods Fluids 7 (1987) 1053–1075.
[27] S.E. Navti, K. Ravindran, C. Taylor, R.W. Lewis, Finite element modelling of surface tension effects using a Lagrangian-Eulerian kinematic description, Comput. Methods Appl. Mech. Eng. 147 (1997) 41–60.
[28] T. Okamoto, M. Kawahara, 3-D sloshing analysis by an arbitrary Lagrangian-Eulerian finite element method, Int. J. Comput. Fluid Dyn. 8 (2) (1997) 129–146.
[29] S. Ushijima, Three dimensional arbitrary Lagrangian Eulerian numerical prediction method for non-linear free surface oscillation, Int. J. Numer. Methods Fluids 26 (1998) 605–623.
[30] A. Soulaimani, Y. Saad, An arbitrary Lagrangian-Eulerian finite element method for solving three-dimensional free surface flows, Comput. Methods Appl. Mech. Eng. 162 (1–4) (1998) 79–106.

[31] J.G. Zhou, P.K. Stansby, An arbitrary Lagrangian-Eulerian σ (ALES) model with non-hydrostatic pressure for shallow water flows, Comput. Methods Appl. Mech. Eng. 178 (1999) 199–214.
[32] L. Gaston, A. Kamara, M. Bellet, An arbitrary Lagrangian-Eulerian finite element approach to non-steady state turbulent fluid flow with application to mould filling in casting, Int. J. Numer. Methods Fluids 34 (4) (2000) 341–369.
[33] H. Braess, P. Wriggers, Arbitrary Lagrangian Eulerian finite element analysis of free surface flow, Comput. Methods Appl. Mech. Eng. 190 (2000) 95–109.
[34] M. Iida, Numerical analysis of self-induced free surface flow oscillation by fluid dynamics computer code SPLASH-ALE, Nucl. Eng. Des. 200 (2000) 127–138.
[35] J. Sung, H.G. Choi, J.Y. Yoo, Time accurate computation of unsteady free surface flows using an ALE-segregated equal order FEM, Comput. Methods Appl. Mech. Eng. 190 (2000) 1425–1440.
[36] M. Souli, J.P. Zolesio, Arbitrary Lagrangian-Eulerian and free surface methods in fluid mechanics, Comput. Methods Appl. Eng. 191 (2001) 451–466.
[37] M.-H. Hsu, C.-H. Chen, W.-H. Teng, An arbitrary Lagrangian-Eulerian finite difference method for computations of free surface flows, J. Hydraul. Res. 39 (2002) 1–11.
[38] S. Rabier, M. Medale, Computation of free surface flows with a projection FEM in a moving framework, Comput. Methods Appl. Mech. Eng. 192 (2003) 4703–4721.
[39] J. Donea, A. Huerta, Finite Element Methods for Flow Problems, John Wiley & Sons, Chichester, 2003.
[40] DC Lo, DL Young, Arbitrary Lagrangian-Eulerian finite element analysis of free surface flow using a velocity-vorticity formulation, J. Comput. Phys. 195 (1) (2004) 175–201.
[41] F. Duarte, R. Gormaz, S. Natesan, Arbitrary Lagrangian-Eulerian method for Navier-Stokes equations with moving boundaries, Comput. Methods Appl. Mech. Eng. 193 (45–47) (2004) 4819–4836.
[42] X. Li, Q. Duan, X. Han, D.C. Sheng, Adaptive coupled arbitrary Lagrangian-Eulerian finite element and meshfree method for injection molding process, Int. J. Numer. Methods Eng. 73 (8) (2008) 1153–1180.
[43] S. Ganesan, L. Tobiska, A coupled arbitrary Lagrangian-Eulerian and Lagrangian method for computation of free surface flows with insoluble surfactants, J. Comput. Phys. 228 (8) (2009) 2859–2873.
[44] P. Nithiarasu, An arbitrary Lagrangian Eulerian (ALE) formulation for free surface flows using the characteristic-based split (CBS) scheme, Int. J. Numer. Methods Fluids 48 (2005) 1415–1428.
[45] J.C. Martin, W.J. Moyce, An experimental study of the collapse of liquid columns on a rigid horizaontal plane, Philos. Trans. R. Soc. Lond. Ser. A 244 (1952) 312–324.
[46] S.R. Idelsohn, N. Calvo, E. Oñate, Polyhedrization of an arbitrary 3D point set, Comput. Methods Appl. Mech. Eng. 192 (2003) 2649–2667.

[47] S.R. Idelsohn, E. Oñate, F. Del Pin, A Lagrangian meshless finite element method applied to fluid-structure interaction problems, Comput. Struct. 81 (2003) 655–671.
[48] S.R. Idelsohn, N. Calvo, E. Oñate, F. Del Pin, The meshless finite element method, Int. J. Numer. Methods Eng. 58 (2003) 893–912.
[49] W.E. Johnson, Development and application of computer programs related to hypervelocity impact, Systems Science and Software, Report 3SR-353, 1970.
[50] R. Codina, U. Schäer, E. Oñate, Mould filling simulation using finite elements, Int. J. Numer. Methods Heat Fluid Flow 4 (1994) 291–310.
[51] K. Ravindran, R.W. Lewis, Finite element modelling of solidification effects in mould filling, Finite Elem. Anal. Des. 31 (1998) 99–116.
[52] R.W. Lewis, K. Ravindran, Finite element simulation of metal casting, Int. J. Numer. Methods Eng. 47 (2000).
[53] J.V. Wehausen, The wave resistance of ships, Adv. Appl. Mech. (1970).
[54] C.W. Dawson, A practical computer method for solving ship wave problems, in: Proceedings of the Second Internatinal Conference on Numerical Ship Hydrodynamics, USA, 1977.
[55] K.J. Bai, J.H. McCarth (Eds.), Proceedings of the Second DTNSRDC Workshop on Ship Wave Resistance Computations, Bethesda, MD, USA, 1979.
[56] F. Noblesse, J.H. McCarthy (Eds.), Proceedings of the Second DTNSRDC Workshop on Ship Wave Resistance Computations. Bethesda, MD, USA, 1983.
[57] G. Jenson, H. Soding, Ship wave resistance computation, in Notes on Numerical Fluid Mechanics, Vol. 25, Vieweg, Brauchschweig, 1989.
[58] Y.H. Kim, T. Lucas, Non-linear ship waves, in: Proceedings of the 18th Symposium on Naval Hydrodynamics, MI, USA, 1990.
[59] D.E. Nakos, P. Sclavounos, On the steady and unsteady ship wave patterns, J. Fluid Mech. 215 (1990) 256–288.
[60] H. Raven, A practical non-linear method for calculating ship wave making and wave resistance, in: Proceedings of the 19th Symposium on Ship Hydrodynamics, Seoul, Korea, 1992.
[61] R.F. Beck, Y. Cao, T.H. Lee, Fully non-linear water wave computations using the desingularized method, in: Proceedings of the 6th Symposium on Numerical Ship Hydrodynamics, Iowa City, Iowa, USA, 1993.
[62] H. Soding, Advances in panel methods, in: Proceedings of the 21st Symposium on Naval Hydrodynamics, Trondheim, Norway, 1996.
[63] C. Janson, L. Larsson, A method for the optimization of ship hulls from a resistance point of view, in: Proceedings of the 21st Symposium on Naval Hydrodynamics, Trondheim, Norway, 1996.
[64] C.C. Mei, H.S. Chen, A hybrid element method for steady linearized free surface flows, Int. J. Numer. Methods Eng. 10 (1976) 1153–1175.
[65] T. Hino, Computation of free surface flow around an advancing ship by Navier-Stokes equations, in: Proceedings of the 5th International Conference on Numerical Ship Hydrodynamics, Hiroshima, Japan, 1989, pp. 103–117.

[66] T. Hino, L. Martinelli, A. Jameson, A finite volume method with unstructured grid for free surface flow, in: Proceedings of the 6th International Conference on Numerical Ship Hydrodynamics, Iowa City, IA, 1993, pp. 173–194.
[67] T. Hino, An unstructured grid method for incompressible viscous flows with free surface, AIAA-97-0862, 1997.
[68] J.H. Duncan, The breaking and non-breaking wave resistance of a two dimensional hydrofoil, J. Fluid Mech. 126 (1983) 507–516.
[69] O.C. Zienkiewicz, R.L. Taylor, J.Z. Zhu, The Finite Element Method: Its Basis and Fundamentals, seventh ed., Elsevier, Oxford, 2013.
[70] S. Giuliani, An algorithm for continuous rezoning of the hydrodynamic grid in arbitrary Lagrangian-Eulerian computer codes, Nucl. Eng. Des. 72 (1982) 205–212.
[71] J. Sarrate, A. Huerta, An improved algorithm to smooth graded quadrilateral meshes preserving the prescribed element size, Commun. Numer. Methods Eng. 17 (2001) 89–99.
[72] J. Hermansson, P. Hansbo, A variable diffusion method for mesh smoothing, Commun. Numer. Methods Eng. 19 (2003) 897–908.
[73] E.V. Laitone, The second approximation to cnoidal and solitary waves, J. Fluid Mech. 9 (1960) 430–444.
[74] T. Maxworthy, Experiments on collisions between solitary waves, J. Fluid Mech. 76 (1976) 177–186.
[75] N. Massarotti, P. Nithiarasu, O.C. Zienkiewicz, Characteristic-based-split algorithm, Part II: Incompressible flow problems with heat transfer, in: K.D. Papailiou et al. (Eds.), Proceedings of the ECCOMAS CFD 1998, vol. 2, Athens, Greece, 1998, pp. 17–21.
[76] N. Massarotti, P. Nithiarasu, O.C. Zienkiewicz, Characteristic-based-split (CBS) algorithm for incompressible flow problems with heat transfer, Int. J. Numer. Methods Heat Fluid Flow 8 (1998) 969–990.
[77] P. Nithiarasu, T. Sundararajan, K.N. Seetharamu, Finite element analysis of transient natural convection in an odd-shaped enclosure, Int. J. Numer. Methods Heat Fluid Flow 8 (1998) 199–220.
[78] R.W. Lewis, P. Nithiarasu, K.N. Seetharamu, Fundamentals of the finite element method for heat and fluid flow, John Wiley and Sons, 2004.
[79] F.P. Incropera, D.P. Dewitt, Fundamentals of Heat and Mass Transfer, third ed., John Wiley, New York, 1990.
[80] A. Bejan, Heat Transfer, John Wiley, New York, 1993.
[81] Y. Jaluria, Natural Convection Heat Transfer, Springer-Verlag, New York, 1980.
[82] O.C. Zienkiewicz, R.H. Gallagher, P. Hood, Newtonian and non-Newtonian viscous incompressible flow, in: J. Whiteman (Ed.), Mathematics of Finite Elements and Applications, vol. II, Academic Press, London, 1976, pp. 235–267.
[83] J.C. Heinrich, R.S. Marshall, O.C. Zienkiewicz, Penalty function solution of coupled convective and conductive heat transfer, in: C. Taylor, K. Morgan, C.A.

Brebbia (Eds.), Numerical Methods in Laminar and Turbulent Flows, Pentech Press, 1978, pp. 435–447.

[84] J.C. Heinrich, C.C. Yu, Finite element simulation of buoyancy driven flow with emphasis on natural convection in horizontal circular cylinder, Comput. Methods Appl. Mech. Eng. 69 (1988) 1–27.

[85] B. Ramaswamy, Finite element solution for advection and natural convection flows, Comput. Fluids 16 (1988) 349–388.

[86] B.V.K. Sai, K.N. Seetharamu, P.A.A. Narayana, Finite element analysis of the effect of radius ratio on natural convection in an annular cavity, Int. J. Numer. Methods Heat Fluid Flow 3 (1993) 305–318.

[87] C. Nonino, S. Del Giudice, Finite element analysis of laminar mixed convection in the entrance region of horizontal annular ducts, Numer. Heat Trans, Part A: Appl. 29 (1996) 313–330.

[88] S.C. Lee, C.K. Chen, Finite element solutions of laminar and turbulent mixed convection in a driven cavity, Int. J. Numer. Methods Fluids 23 (1996) 47–64.

[89] Y.T.K. Gowda, P.A.A. Narayana, K.N. Seetharamu, Finite element analysis of mixed convection over in-line tube bundles, Int. J. Heat Mass Trans. 41 (1998) 1613–1619.

[90] G. De Vahl Davis, Natural convection of air in a square cavity: a benchmark numerical solution, Int. J. Numer. Methods Fluids 3 (1983) 249–264.

[91] P. Le Quere, T.A. De Roquefort, Computation of natural convection in two dimensional cavity with Chebyshev polynomials, J. Comput. Phy. 57 (1985) 210–228.

[92] P. Nithiarasu, N. Massarotti, J.S. Mathur, Forced convection heat transfer from solder balls on a printed circuit board using the characteristic based split (CBS) scheme, Int. J. Numer. Methods Heat Fluid Flow 15 (1) (2005) 73–95.

[93] N. Massarotti, F. Arpino, R.W. Lewis, P. Nithiarasu, Explicit and semi-implicit CBS procedures for incompressible viscous flows, Int. J. Numer. Methods Eng. 66 (10) (2006) 1618–1640.

[94] A. Mauro, P. Nithiarasu, N. Massarotti, F. Arpino, The finite element method: discretization and application to heat convection problems, in: R.S. Amano, B. Sunden (Eds.), Computational Fluid Dynamics and Heat Transfer: Emerging Topics, International Series on Developments in Heat Transfer, WIT Press, Billerica, MA, 2011, pp. 129–170.

[95] F. Arpino, N. Massarotti, A. Mauro, P. Nithiarasu, Artificial compressibility based CBS solutions for double diffusive natural convection in cavities, Int. J. Numer. Methods Heat Fluid Flow 23 (2013) 205–225.